Magnesium Technology 2012
Edited by: Suveen N. Mathaudhu, Wim H. Sillekens, Neale R. Neelameggham, and Norbert Hort
TMS (The Minerals, Metals & Materials Society), 2012

Microstructural Characteristics of High Rate Plastic Deformation in Elektron™ WE43 Magnesium Alloy

Joseph Hamilton[1], Sarah T. Brennan[1], Yongho Sohn[1], Bruce Davis[2], Rick DeLorme[2], Kyu Cho[3]
[1]University of Central Florida; 12443 Research Parkway, Suite 304; Orlando, FL 32826, USA
[2]Magnesium Elektron North America;1001 College St.; P.O. Box 258,; Madison, IL 62060, USA
[3]US Army Research Laboratory; 2800 Powder Mill Rd.; Adelphi, MD 20783, USA

Keywords: Magnesium, High-Strain Rate, Severe Plastic Deformation, Shear Localization

Abstract

High strain rate deformation of WE43 magnesium alloy was carried out by high velocity impacts, and the characteristics and mechanisms of microstructural damage were examined. Six samples were subjected to a variety of high velocity impact loadings that resulted in both partial and full damage. Optical, scanning and transmission electron microscopy analyses were performed in order to identify regions of shear localization. These regions were used to map, both quantitatively and qualitatively, the effects of deformation on the microstructure. Shear localization was observed in every sample, and its depth was measured. Evidence of shear localization was observed to a greater extent in samples with partial damage while fracturing was observed more frequently in samples with full damage.

Introduction

Over the past two decades, there has been an increasing interest in the commercial use of magnesium alloys in various applications where a high strength-to-weight ratio is important, such as in aerospace, automotive, and defense industries [1]. Not only is magnesium an extremely lightweight metal, weighing 30% less than aluminum, and 70% less than steel, it also has the highest strength-to-weight ratio among any of the commonly used non-ferrous and ferrous metallic materials [2].

As magnesium is used more often in structural components, there is an increasing demand for a better understanding of the microstructural evolution during deformation. Due to the limited number of independent slip systems in a hexagonal close packed (HCP) crystal structure, basal slip and twinning are the prevalent mechanism of deformation at lower temperatures, such as 200°C and below, with low strain rates ranging between 1.8×10^{-5} to 1.8×10^{-3} s^{-1} [3]. Wei *et* al., showed that at elevated temperatures ranging from 350 to 425°C, and strain rates ranging from 10^{-3} to 1^{-1} s^{-1}, magnesium alloys exhibited excellent superplasticity, due to activation of non-basal slip systems, and grain boundary sliding (GBS) deformation mechanism under these conditions [4]. It has been noted that as the temperature is increased above 200°C the critical resolved shear stress for the non-basal slip systems is reduced, and the activation of these additional mechanisms results in an increase in ductility and a decrease of yield and flow stress [5]. However, at high strain rates, such as greater than 10^3 s^{-1}, the primary mechanism of deformation in metals has been shown to be shear localization [6] [7].

The shear localization seen in high strain rate deformation is characterized by adiabatic shear bands (ASB). These regions of shear deformation are the result of adiabatic shear, shear instabilities, and shear localization. The main mechanisms of deformation within the ASBs are dynamic recrystallization (DRX), and GBS. It is through these mechanisms that the microstructure accommodates the high kinetic energy seen in severe plastic deformation occurring at high strain rates, such as ~10^3-10^6 s^{-1} [8].

The post-mortem characterization of a deformed microstructure is important to the understanding of the microstructure during deformation, and until a technique is developed that allows real-time diagnostic of the microstructure as it evolves, it will remain as the primary means of investigation of the phenomenon that occur inside shear localization. The purpose of this study was to analyze, through a variety of microscopy techniques, the microstructure of WE43 magnesium alloy samples post-deformation.

Experimental Methods

A post-mortem analysis was performed on six 80mm thick WE43 samples (3.7-4.3% Yttrium, 2.4-4.4% Rare Earths, 0.4% Zirconium, balance Magnesium), that were produced in the T5 condition, thermally quenched after high-temperature rolling, and then artificially aged. The samples were then subjected to high velocity impacts that resulted in varying levels of severe plastic deformation (SPD). The samples were assigned the nomenclature of A, B, and C based on increasing level of damage. The samples were also labeled as Full, or Partial damaged samples based on the extent of SPD. Examples of the cross sectioned regions are shown in Figures 1 and 2.

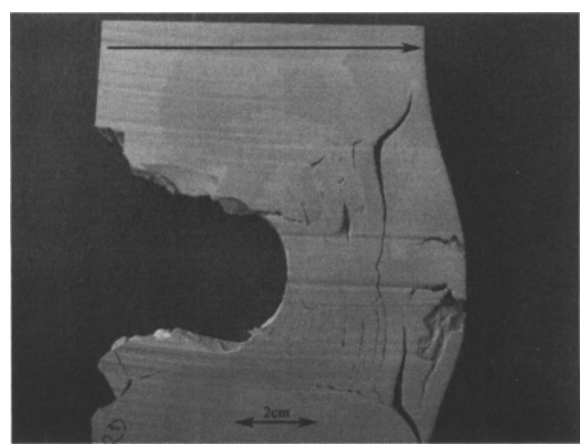

Figure 1. C-Partial sample, after cross sectioning, arrow indicates direction of impact.

In order to preserve the microstructure, preparation methods were chosen that would induce the least amount of damage. Therefore, waterjet cutting was used to cross-section the deformed samples,

and a diamond wafer saw was used to perform further sectioning at low-speed. A map is shown in Figure 3 of the sectioning performed on the sample A-Partial, and this is representative of the method used to section all of the samples. The samples were then mounted in epoxy discs, and mechanically polished to 0.05-μm using alumina. Then the samples were etched by submersion in a acetic-picral etchant (100mL ethanol, 6g picric, 10ml water, 5ml acetic).

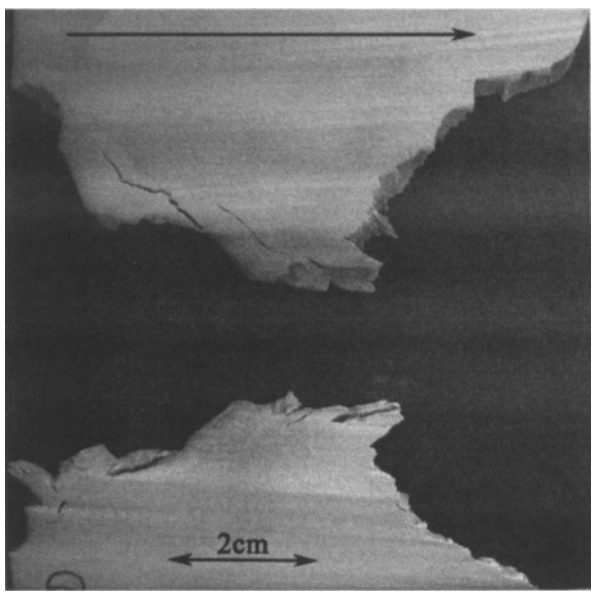

Figure 2. C-Full sample after cross sectioning, arrow indicates direction of impact.

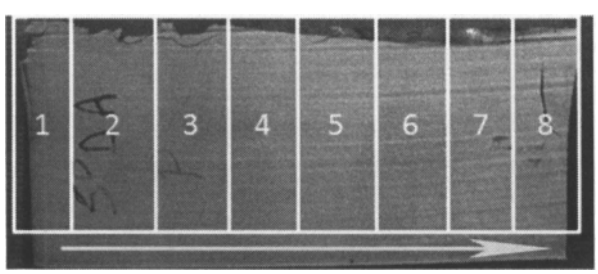

Figure 3. Map of sectioning performed on sample A-Partial, the arrow indicates direction of impact.

In order to characterize different aspects of the deformation a variety of approaches were utilized. Optical microscopy (OM), scanning electron microscopy (SEM), and transmission electron microscopy (TEM) were performed on both deformed and undeformed samples in order to identify and characterize regions of interest.

OM was used for both quantitative and qualitative investigation of shear bands, regions of dynamic recrystallization (DRX), grain size, shear localization, fractures, and damage on the microscale. An Olympus LEXT OLS3000 confocal optical microscope in conjunction with Olympus LEXT software was used for OM imaging. IQ Materials software was used on composite OM images in order to quantify the extent of shear localization. Measurements were made for the depth of the shear localization that extended from the edge of deformation. The regions of deformed and undeformed material were qualitatively distinguished by the features observed with OM. The regions of shear deformation exhibited elongated grains, with shear bands and DRX. The undeformed regions were composed of equiaxed grains and were similar in microstructure to the bulk material. Measurements were taken normal to the edge, across the deformed microstructure, and stopped once an undeformed region was reached, examples of these types of measurements can be seen in Figure 4. The measurements for each sample were averaged, and then the averages for all of the samples were plotted to show the progression of shear localization through the cross-sectioned sample.

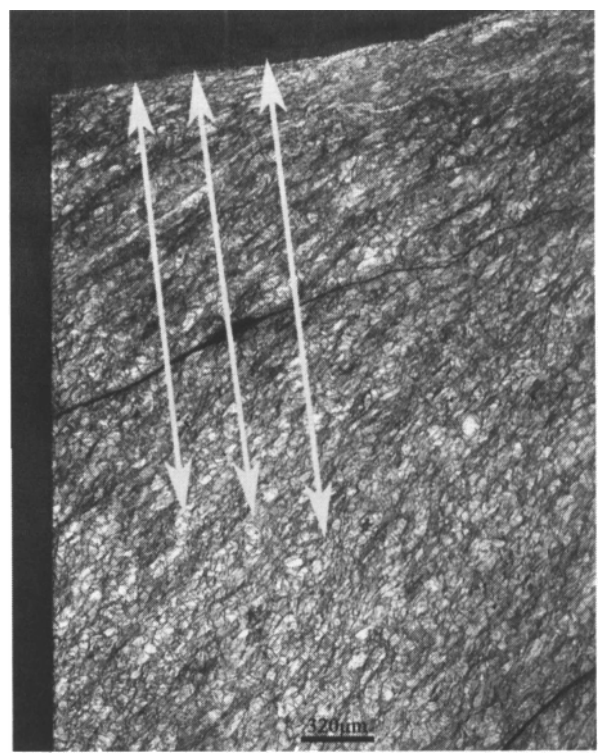

Figure 4. Composite OM image, arrows are example of measurements made of region of shear localization.

SEM was used to further investigate regions of interest at the microscale. A Zeiss Ultra-55 field emission SEM equipped with x-ray energy dispersive spectroscopy (XEDS) was used. TEM was used to investigate the grain size, and formation of precipitates at the nanoscale in regions of DRX found in shear bands, as well as suspected twinning seen throughout the samples. A FEI/Tecnai F30 300keV TEM was utilized for this.

Results and Discussion

Microstructural Characteristics

A section of bulk material was removed and analyzed for comparison to damaged regions. The bulk microstructure (i.e. undamaged) is shown in Figure 5. It was assumed that any twinning, or other characteristics of deformation seen in the bulk

microstructure, was a result of the processing methods used in manufacturing the samples. Although a significant amount of twinning was observed near the surface of the penetration channel, this paper focuses on the shear localization and the formation of shear bands. The presence of profuse twinning was examined by TEM, and will be reported in future publications.

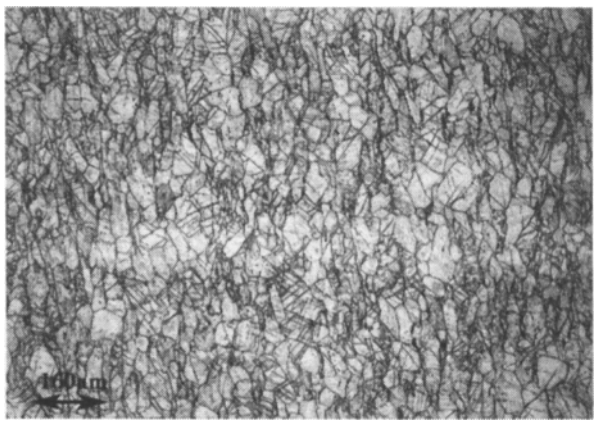

Figure 5. OM of bulk microstructure.

The deformed regions of the samples exhibited a large amount of shear localization, characterized by shear bands and DRX. Shear localization was observed in regions of SPD, and was seen to vary throughout the samples. However, the level of shear localization was highly concentrated in certain areas, and in particular was seen to a greater extent in the Partial-group of samples. These regions were examined further using TEM, and quantified using IQ Materials software.

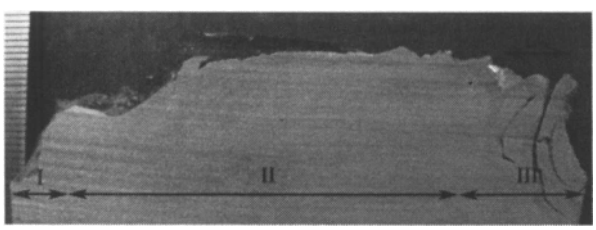

Figure 6. Macroscopic image of the cross-section of sample B-Full, showing microstructural deformation regions I, II, and III

In general, throughout all of the samples, there were three separate regions of distinctive deformation characteristics. Figure 6 shows these regions on the B-Full sample. Region I, the initial area of impact, was characterized by a rough fracture surface along the edge, and a microstructure that was similar to that of the bulk microstructure. An OM of region I is shown in Figure 7. The microstructure of region II showed extensive shear localization, with ASB, DRX, and a smooth edge along the channel as presented in Figure 8. Similar to Region I, region III was composed of a microstructure very similar to that of the bulk microstructure, however, there is a large amount of shear fracturing along the edge. Figure 9 shows the microstructure of region III. The Partial-damage samples did not have a region III, but instead were composed of regions I and II, except in the case of C-Partial which exhibited a large amount of bulging petal fractures.

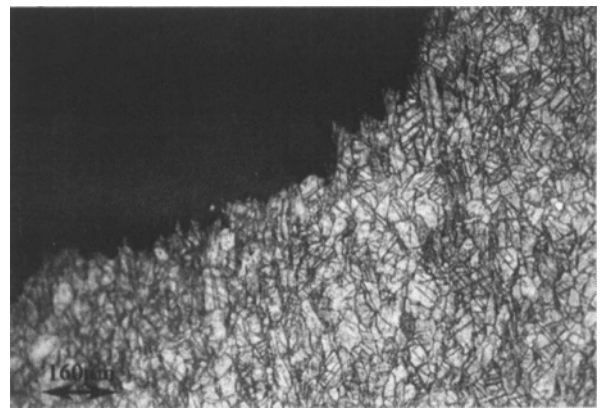

Figure 7. OM image showing typical microstructure of region I.

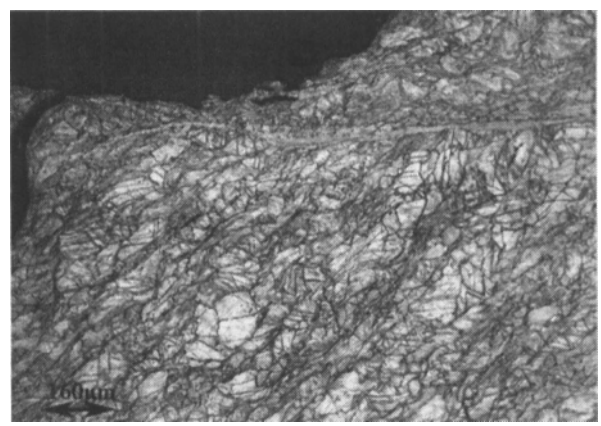

Figure 8. OM image showing shear localization that characterized region II.

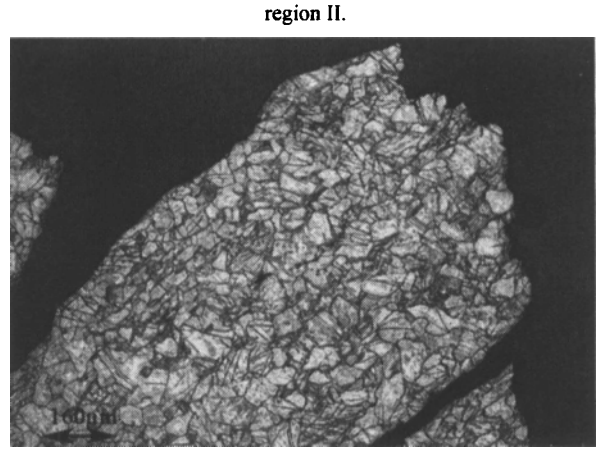

Figure 9. OM image of region III, similar fracture edge and microstructure to that of Region I.

The major variation in these regions, as seen when comparing between each of the sample sets, was the overall size of the regions. Of all of the sample sets, those in sample set A showed the smallest regions I and III, while sample set C showed the largest. As regions I and III were composed of large quantities of shear fracture surfaces, it is likely the higher level of energy transferred during the impacts for sample set C were the largest,

thus resulting in a greater amount of shear fracturing instead of localized shear deformation.

Shear Localization Depth

Shear localization was present in every deformed cross-sectioned sample. In order to appreciate the extent of shear localization, composite OM images were formed, and the region of shear deformation was measured using IQ Materials software. Each sectioned sample (as shown in Figure 3 for sample A-Partial), of both the Partial and Full samples of each sample set was analyzed. The measurements for each sample were averaged, and the plots are presented in Figures 10, 11, and 12.

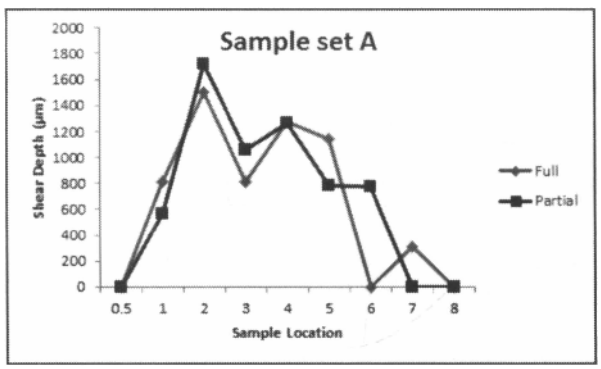

Figure 10. Shear localization depth of sample set A.

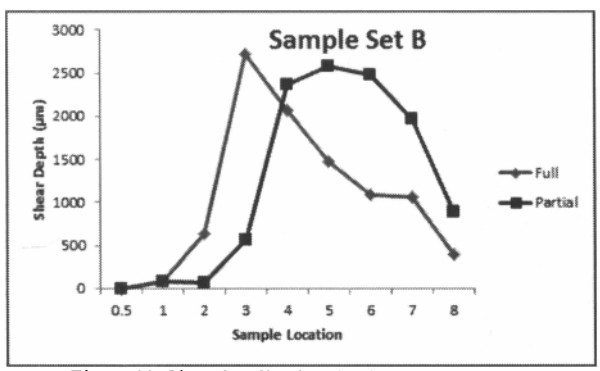

Figure 11. Shear localization depth of sample set B.

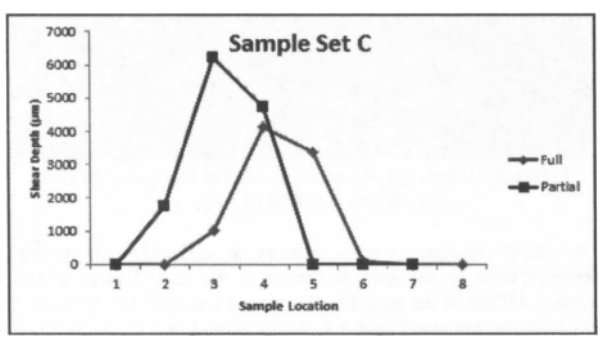

Figure 12. Shear localization depth of sample set C.

Sample set A exhibited a similar quantity of shear localization in both the Full and Partial samples. Furthermore, the overall magnitude of shear depth was to a much lesser degree than either the B or C samples which were both subjected to a much greater level of plastic deformation. The lower level of shear present in sample set A was a result of the lower level of kinetic energy transferred from the high velocity impact.

In sample set B, there was a marked difference in the level of shear localization present in the Partial sample, when compared to the Full sample. Overall, the Partial sample exhibited a greater amount of shear localization, as can be seen in locations 5-8 of Figure 12. In the Full sample, in the regions of lower shear localization, there was a high level of shear fracturing observed.

The greatest magnitude of shear localization was measured in sample set C, as was expected due to the gross amount of severe plastic deformation observed. Of note, the sample locations 5, 6, and 7 of the Partial sample were positioned in such a way, in relation to the damaged edge, to make it impractical to measure shear depth. However, qualitatively these samples had a low amount of shear localization, and there was an extensive amount of fracturing observed, as can readily be seen on a macroscopic level on the right side of the sample in Figure 13.

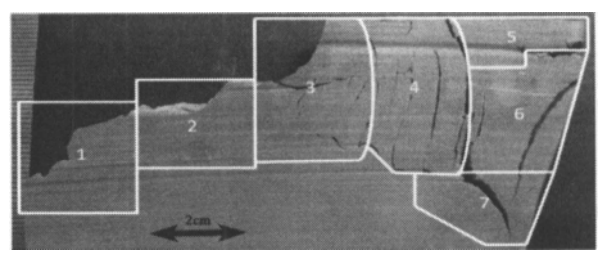

Figure 13. Map of sectioned samples of C-Partial

Overall, shear localization was seen to the greatest extent in the Partial sample group. The shear localization is a result of the microstructure of the material accommodating the kinetic energy from the high velocity impact. When the kinetic energy exceeded a certain amount, full penetration of the sample would occur, and this was characterized by a much higher level of fracturing in the microstructure. Below that level, the material would accommodate the kinetic energy not by fracturing, but instead by shear localization.

A limitation of this study is that any region of the sample that was completely fractured away was no longer attached to the sample, and as a result, not available for post-mortem analysis. It is possible that shear localization was present in these portions of the sample, but no analysis was able to be performed.

Adiabatic Shear Bands

Adiabatic shear bands were a ubiquitous characteristic of regions of shear localization. The shear bands were composed of areas of DRX, which is a result of adiabatic temperature rise [8]. Both regions of DRX, and the transition zone between the DRX and neighboring microstructure, were examined by TEM. The shear band that was analyzed is shown in Figure 14.

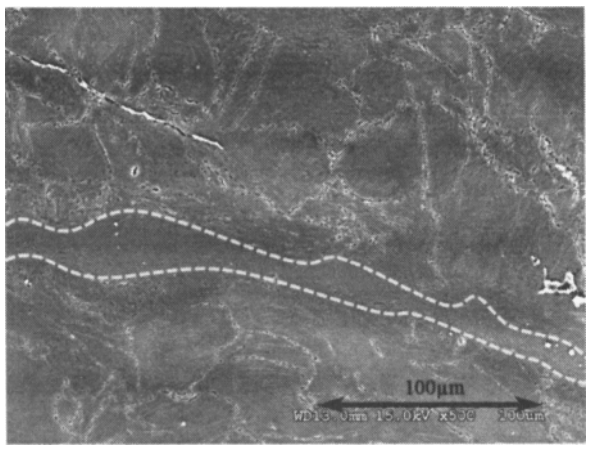

Figure 14. SEM-SE image, with dotted outline of the region of DRX within shear band, that was analyzed by TEM.

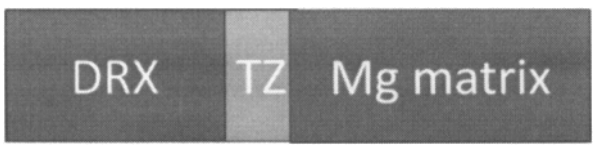

Figure 15. Diagram of shear band, and neighboring microstructure.

The shear band was composed of two distinct regions as schematically illustrated in Figure 15. The first region of DRX was composed of small equiaxed recrystallized grains (<500nm) that contained a very limited amount of precipitates, while the second region was a transition zone (TZ) that contained both the larger grains of the bulk matrix, and the smaller grains similar in size to the DRX region. The TEM of the DRX region is shown in Figure 16, while that of the TZ region is shown in Figure 17.

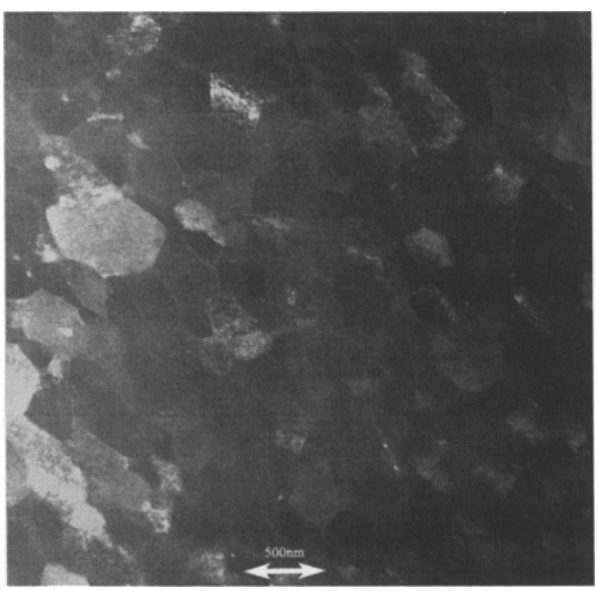

Figure 16. TEM image of DRX region of shear band.

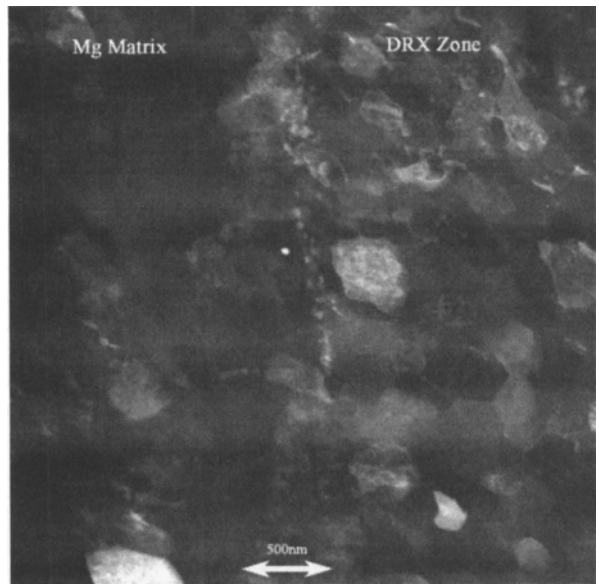

Figure 17. TEM image of transition zone interfacing the DRX region and neighboring microstructure.

The neighboring matrix was similar to that of the bulk material shown in Figure 18, containing large grains with smaller precipitates, and smaller grain regions with large secondary phase precipitates. Indexing performed on the diffraction pattern from a large secondary phase precipitate showed that it was β phase: $Mg_{14}Nd_2Y$ (fcc, a = 2.223nm). Figure 19 shows the diffraction pattern.

Figure 18. TEM image of bulk microstructure, the large precipitate that was indexed is marked.

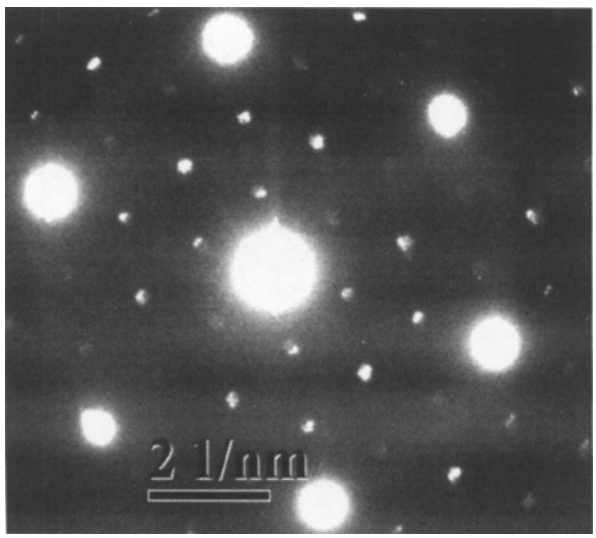

Figure 19. Diffraction pattern of large precipitate found in small grain region of bulk material, indexing to be β phase.

The smaller precipitates located in the coarse grains were analyzed by XEDS as shown in Figure 20, and the composition was quantified as $Mg_{74.8}Y_{17.2}Nd_{8.0}$ (at%). This suggests that these percipitates are most likely β" phase: $Mg_3(Y_{0.85}Nd_{0.15})$.

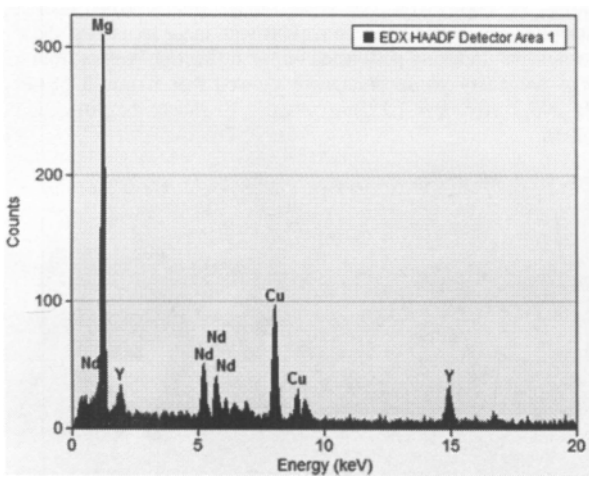

Figure 20. XEDS results of smaller precipitates contained in coarse grains of bulk microstructure.

Conclusions

After a set of six WE43 magnesium alloy samples were subjected to different high-velocity impacts, which resulted in high-strain rate severe plastic deformation, the microstructures of the deformed samples were analyzed and compared to the bulk material. Shear localization, characterized by bands of dynamic recrystallization, was seen throughout the damaged regions. However, samples that were subjected to impacts that resulted in only partial damage were seen to have a larger quantity of shear localization, compared to those samples that experienced impacts that resulted in full damage. Furthermore, the samples with full damage had a lower occurrence of shear localization in the regions of high shear fracture. This indicates that the material would accommodate the lower level of kinetic energy, which was insufficient to result in shear fracture, by shear localization in the microstructure.

The regions of shear localization, when analyzed by TEM showed distinct variation from the bulk material microstructure. The bulk material was composed of regions with coarse grains containing small elongated precipitates of the β" phase, and smaller grain regions with large β phase precipitates. Microstructure within the ASB was distinctively different. The shear bands were composed of small (<500nm) grains, with a very limited amount of precipitates. In addition, there was a transition zone between the two regions that showed a mixture of both the larger grains seen in the bulk material, and the smaller grains seen in the region of DRX.

Acknowledgements

Research was sponsored by US Army Research Laboratory and was accomplished under Cooperative Agreement W911NF-07-2-0073. The views, opinions, and conclusions made in this document are those of the authors and should not be interpreted as representing the official policies, either expressed or implied, of Army Research Laboratory or the US Government. The US Government is authorized to reproduce and distribute reprints for Government purposes notwithstanding any copyright notation herein.

Works Cited

[1] B. Mordike T. Ebert, "Magnesium Properties - applications - potential," *Materials Science and Engineering A*, vol. 302, no. 1, pp. 37-45, 2001.

[2] *Magnesium Die Casting Handbook*. New York, USA: NADACA, 1998.

[3] M. Janecek, P. Dobron, F. Chmelik, V. Supik, F. Hollander R. Kral, "Mechanisms of plastic deformatoin in AZ31 magnesium alloy investigated by acoustic emission and transmission electron microscopy," *Materials Science and Engineering A*, vol. 462, no. 1-2, pp. 311-315, 2007.

[4] Y.H. Wei, Y.P. Zhu, H.T. Zhou, W.J. Ding, Y. Chino, M. Mabuchi Q.D. Wang, "Superplasticity and grain boundary sliding in rolled AZ91 magnesium alloy at high strain rates," *Materials Science and Engineering A*, vol. 360, no. 1-2, pp. 107-115, 2003.

[5] S. Agnew, Ö. Duygulu, "Plastic anisotropy and the role of non-basal slip in magnesium alloy AZ31B," *International Journal of Plasticity*, vol. 21, no. 6, pp. 1161-1193, 2005.

[6] M. Meyers, "Shear localization in dynamic deformation of materials: microstructural evolution and self-organization," *Materials Science and Engineering A*, vol. 317, no. 1-2, pp. 204-225, 2001.

[7] C.W. Tan, L. Wang, Z.Y. Chen, F. Wang, H. Cai, H.L. Ma S. Xu, "Deformation behavior of AZ31 magnesium alloy at different strain rates and temperatures," *Trans. Nonferrous Met. Soc. China*, vol. 17, pp. S347–S352, 2007.

[8] L. Murr, S. Pappu, C. Kennedy E. Trillo, "Adiabatic shear bands and examples of their role in severe plastic deformation," *Journal of Materials Science*, vol. 37, no. 16, pp. 3337–3360, 2002.